

Running title: Liquid Breakup Models for High-Pressure Dense Diesel Sprays

Front. Energy

DOI 10.1007/s11708-000-0000-0

RESEARCH ARTICLE

Assessment and Validation of Liquid Breakup Models for High-Pressure Dense Diesel Sprays

Yi Ren and Xianguo Li*

Department of Mechanical and Mechatronics Engineering
University of Waterloo, Waterloo, Ontario, Canada

* Corresponding author, Xianguo.Li@uwaterloo.ca

Abstract Liquid breakup in fuel spray and atomization significantly affects the consequent mixture formation, combustion behavior, and emission formation processes in a direct injection diesel engine. In this study, various models for liquid breakup processes in high-pressure dense diesel sprays and its impact on multi-dimensional diesel engine simulation have been evaluated against experimental observations, along with the influence of the liquid breakup models and the sensitivity of model parameters on diesel sprays and diesel engine simulations. It is found that the modified Kelvin-Helmholtz (KH) – Rayleigh-Taylor (RT) breakup model gives the most reasonable predicted results in both engine simulation and high-pressure diesel spray simulation. For the standard KH-RT model, the model constant C_{bl} for the breakup length has a significant effect on the model's predictability, and a fixed value of the constant C_{bl} cannot provide a satisfactory result for different operation conditions. The Taylor-Analogy-Breakup (TAB) based models and the RT model do not provide reasonable predictions for the characteristics of high-pressure sprays and simulated engine performance and emissions.

Keywords: breakup model, diesel engine, high-pressure injection, simulations

1. Introduction

High-pressure direct injection diesel engine is becoming popular for high-performance low emission automotive applications. It has been demonstrated that liquid fuel atomization and spray formation is one of the key in-cylinder processes affecting combustion and emission characteristics, the improvement of thermal efficiency and reduction of exhaust emissions are achieved through optimizing fuel spray characteristics and injection strategy. Badami et al. [1] studied the impact of the injection pressure on the performance of a direct injection (DI) diesel engine with a high-pressure common rail system. They found that high-pressure injection results in the increase in the maximum power, and the reduction in the soot formation and fuel consumption. The influence of the discharge nozzle hole geometry of a diesel injector was studied by Pontoppidan et al. [2]. They found that the optimized injector geometry would produce a better exhaust performance. Felice et al. [3] investigated the potential of the multiple injection strategy for the achievement of low emissions in a high-pressure direct injection diesel engine. It was demonstrated that using the multiple injection strategy reduces peak heat release rate, and NO_x and smoke exhaust emissions.

In recent years, multi-dimensional computational fluid dynamics (CFD) simulation of in-cylinder processes has become the tool for engine design and optimization, in response to the enforcement of more and more stringent emission regulations. In DI diesel engines, liquid fuel is injected directly into the combustion chamber where it will break up into individual droplets, eventually vaporize and ignite. Spray droplets may undergo a number of processes from the time they are injected until the time of complete vaporization. Thus, a series of spray sub-models need to be implemented to simulate the diesel dense spray processes including drop breakup, collision, evaporation, and so forth. Significant efforts have been made to develop various spray sub-

models for incorporation into CFD simulation. Reitz [4, 5] presented the wave breakup theory using the development of Kelvin-Helmholtz (KH) instabilities on a jet surface. The Rayleigh-Taylor (RT) breakup model was developed based on the theoretical considerations of Taylor [6, 7]. The KH-RT hybrid breakup model consists of both Kelvin-Helmholz and Rayleigh-Taylor instability theories, and it is expected to have a greater potential than previous models to provide enhanced simulation results [8]. O'Rourke et al. [9] presented the Taylor-Analogy-Breakup (TAB) model based on the assumption that droplet distortion can be described as a spring-mass system. They also developed the extensions of a three-dimensional computational model for the liquid wall films formed in port-injected engines, and the computed film locations agree qualitatively with those observed in laser-induced fluorescence measurements [10]. Moreover, Schmidt et al. presented a numerical collision scheme named the No Time Counter (NTC) method [11].

However, in spite of these many efforts, the spray simulation is not sufficiently accurate to advance fuel injection strategies and spray characteristics to the point that engines can be developed solely based on the CFD simulation that can comply with ever-stricter emission standards. On one hand, simulation results may vary considerably, depending on the details of the submodels implemented. On the other hand, the complexities of the spray processes must be included and dealt with in the spray submodels. Therefore, it is essential to assess the validity and accuracy of the previously developed models for a variety of conditions that may be encountered in high-pressure direct injection diesel engines. Sone et al. [12] investigated the effect of sub-grid modeling on an in-cylinder unsteady mixing process in a direct injection engine. In their study, the predicted results of an in-cylinder turbulent fuel-air mixing process were found to be significantly sensitive to their turbulence model. The large eddy simulation for

both non-evaporative and evaporative diesel spray was implemented by Hori et al. [13] in a constant volume vessel. Larimi et al. [14] conducted a medium speed diesel engine simulation, and found that the fuel viscosity effect on drop sizes was well predicted by a KH-RT breakup model. Moreover, Fujimoto et al. [15] studied the predictive capability of various spray breakup models on a non-evaporative diesel spray. Their results show that for a non-evaporative diesel spray simulation, the breakup model significantly affects the calculated spray shape.

Liquid breakup models play a key role in a spray CFD simulation. Therefore, in the current study, numerical studies on the evaporative diesel-like fuel spray have been conducted in an attempt to assess the accuracy of the existing spray breakup models which are widely used in diesel engine simulations. The effect of liquid breakup models and the sensitivity of the model parameters on the simulation of diesel fuel spray characteristics are highlighted by comparing the numerical results against experimental data available in literature. Meanwhile, the performance of the spray breakup models is analyzed for high-pressure diesel spray simulations. In addition, a diesel engine simulation is also implemented and compared with experimental measurements to enhance the understanding of the effect of spray breakup models on engine CFD simulations for high-pressure direct injection diesel engines.

2 Experimental

2.1 Spray

In this study, the experimental data used for the assessment and validation of spray breakup models are taken from [16]. The spray was injected under high pressure into a constant volume vessel, which was used to create the high pressure and high temperature ambient condition. Inert gas, sulfur hexafluoride (SF₆), was charged into the vessel as the working medium and was

heated by burning the mixture of H₂ and O₂ inside the vessel. The temperature and density of the gas in the vessel ranged 800-1100 K and 20-100 kg/m³, respectively. A mixture of n-decane, naphthalene (NP) and tetramethyl-p-phenylene diamine (TMPD) by mass proportion of 90:9:1 was used to substitute for diesel fuel and injected into the vessel by an electronically controlled single-hole injector. The experimental condition included the injection pressure of 180 MPa, the injection duration of 1.0 mm and the injector diameter D_n of 0.1 mm. The equivalence ratio of the vapour-phase spray in the vessel was measured quantitatively using planar laser induced exciplex fluorescence (PLIEF) technique. Before fuel injection, SF₆, H₂, and O₂ were charged into the vessel and ignited by a spark plug to create the high temperature and high pressure environment. Injection started when the ambient temperature dropped to the pre-set value. During the experiment, the ambient pressure was measured using a Kistler 6125B type pressure sensor. Further details of the experiment are referred to [16].

2.2 Engine

In order to further increase the understanding of the predictive capability of the breakup models, a 3D engine simulation is also performed, and the simulated results are compared to another experimental measurement of engine tests. This experiment was conducted by Klingbeil et al. [17] on a Caterpillar 3401E single cylinder oil test engine (SCOTE). The engine specifications are listed in Table 1. Its fuel injector was a production style Caterpillar electronic unit injector. The characteristics of the injection system are given in Table 2.

3. Model Formulation

3.1 Governing Equations

In the numerical simulation study, the dynamics of the fluid flow within the cylinder of a direct injection diesel engine and the constant-volume vessel are governed by the compressible

equations for the conservation of mass, momentum, energy and species. In these equations, the Einstein's tensor notation is utilized for multi-dimensional flow. Considering the turbulent flow, the flow property N (u_i , h , e , T , and Y_m) is decomposed by the Reynolds averaging as follows [26]:

$$N = \bar{N} + N' \quad (1)$$

$$\overline{N'} \equiv 0 \quad (2)$$

where \bar{N} is a time-averaged component and N' is a fluctuating component; and the flow property M (p , q , and ρ) is decomposed by the Favre averaging as follows:

$$M = \tilde{M} + M'' \quad (3)$$

$$\tilde{M} \equiv \frac{\bar{\rho}M}{\bar{\rho}} \quad (4)$$

For the Favre averaging, where \tilde{N} is a mass-averaged component and N'' is a fluctuating component.

The variables given above mean that u_i is the instantaneous velocity in the direction x_i , e is the specific internal energy, T is the temperature, h is the specific enthalpy, Y_m is the mass fraction of the species m , p is the pressure, q is the heat-flux vector, and ρ is the density.

The governing equations considering the compressible turbulent flow are expressed as follows:

Conservation of Mass:

$$\frac{\partial \bar{\rho}}{\partial t} + \frac{\partial}{\partial x_i} (\bar{\rho} \tilde{u}_i) = S_n \quad (5)$$

where S_n is the mass source term derived from the evaporation of the injected fuel.

Conservation of Momentum:

$$\frac{\partial \bar{\rho} \tilde{u}_i}{\partial t} + \frac{\partial}{\partial x_j} (\bar{\rho} \tilde{u}_j \tilde{u}_i) = -\frac{\partial \bar{p}}{\partial x_i} + \frac{\partial}{\partial x_j} [\bar{\sigma}_{ji} - \tau_{ji}] + S_j \quad (6)$$

where σ_{ji} is the stress tensor, τ_{ji} is the Reynolds stress tensor, S_j is the source term arises from fuel spray and gravitational acceleration.

Conservation of Energy:

$$\frac{\partial}{\partial t} \left[\bar{\rho} \left(\tilde{e} + \frac{1}{2} \tilde{u}_i \tilde{u}_i \right) \right] + \frac{\partial}{\partial x_j} \left[\bar{\rho} \tilde{u}_j \left(\tilde{h} + \frac{1}{2} \tilde{u}_i \tilde{u}_i \right) \right] = \frac{\partial}{\partial x_j} \left(-\bar{q}_j + \tilde{u}_i \bar{\sigma}_{ji} \right) - \frac{\partial}{\partial t} \left(\frac{1}{2} \bar{\rho} \overline{u_i'' u_i''} \right) + \quad (7)$$

$$\frac{\partial}{\partial x_j} \left(-\tilde{u}_j \tau_{ji} + \frac{1}{2} \tilde{u}_j \overline{u_i'' u_i''} - \frac{\mu_t c_p}{Pr_t} \frac{\partial \tilde{T}}{\partial x_j} \right) + S_e$$

where $e = c_v T$; $q_j = -k \frac{\partial T}{\partial x_j} = -\frac{\mu}{Pr} \frac{\partial h}{\partial x_j}$; μ_t is the turbulent viscosity; c_p is the specific heat at constant pressure; c_v is the specific heat at constant volume; Pr_t is the turbulent Prandtl number, $Pr_t = \frac{c_p \mu_t}{k}$; k is the thermal conductivity; S_e represents the source from chemical reactions and turbulent dissipation.

Conservation of Species:

$$\frac{\partial \bar{\rho} \tilde{Y}_m}{\partial t} + \frac{\partial}{\partial x_j} (\bar{\rho} \tilde{u}_j \tilde{Y}_m) = -\frac{\partial \bar{J}_j^m}{\partial x_j} - \frac{\partial \bar{\rho} u_j'' Y_m''}{\partial x_j} + S_m \quad (8)$$

where m represents the individual chemical species in the fluid mixture, and S_m is the species source term derived from the chemical reactions and fuel evaporation. The diffusion flux is given by

$$\bar{J}_j^m = -\bar{\rho} D_m \frac{\partial \tilde{Y}_m}{\partial x_j} \quad (9)$$

in which D_m is the mass diffusion coefficient for the species m ,

$$\bar{\rho} u_j'' Y_m'' = -\frac{\mu_t}{Sc_t} \frac{\partial \tilde{Y}_m}{\partial x_j} \quad (10)$$

The stress tensor, σ_{ji} , is given as

$$\bar{\sigma}_{ji} = \mu_t \left(\frac{\partial \tilde{u}_i}{\partial x_j} + \frac{\partial \tilde{u}_j}{\partial x_i} \right) - \frac{2}{3} \mu_t \frac{\partial \tilde{u}_k}{\partial x_k} \delta_{ij} \quad (11)$$

The Reynolds stress tensor, τ_{ji} , is given as

$$\tau_{ji} = -\overline{\rho u_i'' u_j''} = \mu_t \left(\frac{\partial \tilde{u}_i}{\partial x_j} + \frac{\partial \tilde{u}_j}{\partial x_i} \right) - \frac{2}{3} \left(\overline{\rho} \kappa + \mu_t \frac{\partial \tilde{u}_i}{\partial x_i} \right) \delta_{ij} \quad (12)$$

where δ_{ij} is the Kronecker delta, and the turbulent kinetic energy, κ , is given by $\kappa = \frac{1}{2} \overline{u_i'' u_i''}$. The turbulent kinetic energy is obtained using the turbulence model which is described in the subsection of turbulence model later on.

3.2 Breakup models

To model the breakup of the injected liquid bulk, the Kelvin-Helmholtz (KH) model, the Rayleigh-Taylor (RT) and the Taylor Analogy Breakup (TAB) models are widely used in 3D engine simulations.

3.2.1 Kelvin-Helmholtz (KH) breakup model

The Kelvin-Helmholtz instability is based on a liquid jet stability analysis that is described in detail by Reitz [4, 5]. The analysis considers the stability of a cylindrical, viscous, liquid jet with an initial radius r_0 which is penetrating into an incompressible, inviscid gas with a relative velocity u_{rel} . It is also assumed that the turbulence generated inside the nozzle hole results in the presence of a spectrum of sinusoidal waves on the liquid jet surface. These surface waves have an infinitesimal axisymmetric displacement initially, and grow due to aerodynamic forces derived from the relative velocity between the liquid and gas. As shown in Fig. 1(a), it is assumed that the new droplet size is proportional to the maximum wavelength, Λ_{KH} , and the change rate of the droplet size is given as:

$$\frac{dr}{dt} = \frac{r - r_{new}}{\tau_{KH}} \quad (13)$$

where τ_{KH} is the KH model breakup time and r_{new} is the radius of the new droplet, they are described as:

$$\tau_{KH} = \frac{3.726 B_1 r}{\Lambda_{KH} \Omega_{KH}} \quad (14)$$

$$r_{new} = B_0 \cdot \Lambda_{KH} \quad (15)$$

where $B_0 = 0.61$, B_1 is an adjustable model constant, Ω_{KH} is the maximum growth rate.

3.2.2 Rayleigh-Taylor (RT) breakup model

The Rayleigh-Taylor instability mechanism as shown in Fig. 1(b) considers that the unstable RT waves occur because of the rapid deceleration of the drops which arises from the aerodynamic drag force F_{aero} :

$$F_{aero} = \pi r^2 c_D \frac{\rho_g u_{rel}^2}{2} \quad (16)$$

Dividing the drag force by the mass of the drop, the acceleration of the interface can be expressed as

$$a = \frac{3}{8} c_D \frac{\rho_g u_{rel}^2}{\rho_l r} \quad (17)$$

where c_D is the drag coefficient of the drop, and r is the radius of the drop.

The new droplet radius, r_{RT} , and the model breakup time, τ_{RT} , are given as:

$$r_{RT} = 0.5 \Lambda_{KH} \quad (18)$$

$$\tau_{RT} = \Omega_{RT}^{-1} \quad (19)$$

3.2.3 KH-RT hybrid breakup model

A single model is usually not able to describe well the whole breakup process of the engine sprays. Hence in this study, the KH-RT hybrid breakup model is implemented to simulate the diesel breakup, as in the work of Senecal [7]. The droplet breakup modeled by the RT model is too fast if such model is implemented at the nozzle hole [2]. Therefore, in this model, KH mechanism is responsible for drop breakup before the breakup length L_b , while both KH and RT mechanisms are activated beyond L_b as shown in Figure 1(c). Firstly, it is checked if the RT mechanism can break up the droplet. If not, the KH mechanism will be responsible for breakup.

The breakup length, L_b , of the injected diesel fuel jet is calculated by

$$L_b = d_0 C_{bl} \sqrt{\frac{\rho_l}{\rho_g}} \quad (20)$$

where d_0 is the nozzle diameter, ρ_l and ρ_g are the ambient gas density and droplet density, respectively. The breakup length constant C_{bl} can be tuned from 0 to 50. In this study, C_{bl} is set to 0, 10 and 40, respectively, in order to assess its impact on the results of the spray simulation.

Further, as an alternative to the KH-RT breakup model, the modified KH-RT model is also implemented in this study. In this model, the specific breakup length L_b is removed. Instead, the KH model is responsible for the primary breakup of the injected “Parent” liquid blobs, during which “Child” drops are created. Thus, the secondary breakup of these drops is modeled by examining the competing effects of the KH and RT mechanisms.

3.2.4 Taylor-Analogy-Breakup (TAB) model

TAB breakup model is a classic method of calculating drop distortion and breakup. This method was developed based on Taylor’s analogy between an oscillating and distorting droplet and a spring-mass system [9]. In the TAB model, the breakup drop radius r is able to be calculated both with and without a drop size distribution. For the model without the drop size distribution, the new droplet radius r' is determined as follows:

$$r' = \frac{r_0}{1 + \frac{8K}{20} + \frac{\rho_l r_0^3}{\sigma} \dot{y}^2 \left(\frac{6K - 5}{120} \right)} \quad (21)$$

where r_0 is the particle radius before breakup; \dot{y} is the velocity of the parameter y , $y = 2x/r_0$, which is the non-dimensional displacement of the particle surface; x is the displacement of the drop equator from its equilibrium position; K is the ratio of the distorting energy of a particle to its total energy; σ is the surface tension of the particle.

In the TAB model with a drop size distribution, eq. (21) provides the Sauter Mean Radius r_{32} ($r' = r_{32}$). The chi-squared and the Rosin-Rammler distribution may be used in the TAB model, respectively. For the chi-squared distribution, the probability density function is given by:

$$C(r) = \frac{1}{\bar{r}} \exp\left(-\frac{r}{\bar{r}}\right) \quad (22)$$

where r is the drop radius and \bar{r} is the number averaged drop radius given by

$$\bar{r} = \frac{1}{3} r_{32} \quad (23)$$

For the Rosin-Rammler distribution, the probability density function is described as:

$$R(r) = 1 - \exp\left(-\frac{r^a}{q}\right) \quad (24)$$

where a and q are empirical model constants.

In this study, all the above breakup models, including the modified KH model, the KH-RT hybrid models with various breakup lengths, the TAB model (without the drop size distribution), TAB-CHI model (with the chi-squared drop size distribution), TAB-RR model (with the Rosin-Rammler drop size distribution) are implemented and their impact on the spray characteristics are investigated.

3.3 Turbulence Modeling

Turbulence directly influences fuel injection and atomization processes, spray characteristics, mixing and combustion processes in an internal combustion engine, thereby, the turbulence model plays an important role in internal combustion engine simulations. The rapid distortion RNG $k-\varepsilon$ model was developed by Han et al. [18] based on the standard $k-\varepsilon$ [19] and RNG $k-\varepsilon$ models [20]. And its superiority has been demonstrated earlier [21]. Hence, the rapid distortion RNG $k-\varepsilon$ turbulence model is applied in this study.

The transport equation for the turbulent kinetic energy, k , of the rapid distortion RNG k - ε model developed by Han et al. [18] is given as

$$\frac{\partial \bar{\rho} k}{\partial t} + \frac{\partial (\bar{\rho} \tilde{u}_j k)}{\partial x_j} = \tau_{ij} \frac{\partial \tilde{u}_i}{\partial x_j} + \frac{\partial}{\partial x_j} \left(\frac{\mu_t}{P_r} \frac{\partial k}{\partial x_j} \right) - \bar{\rho} \varepsilon + S_s \quad (25)$$

where ε is the dissipation of turbulent kinetic energy and S_s is the source term. μ_t is the turbulent viscosity and P_r is the Prandtl number, and τ_{ij} is the Reynolds stress.

Considering the interactions of turbulence with the discrete phase, the source term S_s includes the fluctuating component of the gas-phase velocity as below

$$S_s = - \frac{\sum N_p (F'_{drag,i} u''_i)_p}{V} \quad (26)$$

where the summation is over all parcels in a grid cell, N_p is the number of the drops in a parcel, V is the cell volume, and F'_{drag} is defined by

$$F'_{drag,i} = \frac{F_{drag,i}}{(\bar{u}_i + u'_i - v_i)} u''_i \quad (27)$$

where $F_{drag,i}$ is the drag force on a drop and v_i is a drop velocity.

The transport equation of the dissipation of turbulent kinetic energy, ε , is given by

$$\begin{aligned} \frac{\partial \bar{\rho} \varepsilon}{\partial t} + \frac{\partial \bar{\rho} \tilde{u}_j \varepsilon}{\partial x_j} = \frac{\partial}{\partial x_j} \left(\frac{\mu_t}{P_r} \frac{\partial \varepsilon}{\partial x_j} \right) - \left[\frac{2}{3} C_1 - C_3 + \frac{2 C_\mu \eta (1 - \eta/\eta_0) k}{3 (1 + \beta \eta^3)} \frac{\partial \tilde{u}_k}{\varepsilon \partial x_k} \right] \bar{\rho} \varepsilon \frac{\partial \tilde{u}_i}{\partial x_j} \\ + \left[\left(C_1 - \frac{\eta (1 - \eta/\eta_0)}{(1 + \beta \eta^3)} \right) \frac{\partial \tilde{u}_i}{\partial x_j} \bar{\sigma}_{ij} - C_2 \bar{\rho} \varepsilon + C_s S_s \right] \frac{\varepsilon}{k} \end{aligned} \quad (28)$$

where the model constants β , C_1 , C_2 , C_3 , C_μ and C_s are 0.012, 1.42, 1.68, -1.0, 0.0845 and 1.5, respectively. η is given by $\eta = \frac{k}{\varepsilon} \cdot |S_{ij}|$ in which S_{ij} is the mean strain rate tensor.

The other sub-models used in this study are listed in Table 3.

4 Computational Grids

In this study, the numerical simulation is implemented using the Converge™ CFD code. It is well known that spray simulation is sensitive to the resolution of the numerical grids used. In this study, in order to reduce the grid dependency, the original grid resolution of 2.0×2.0 mm is refined to 1.0×1.0 mm and 0.5×0.5 mm. The adaptive mesh refinement (AMR) technique is also implemented to refine the grid to a minimum of 0.25×0.25 mm. During the simulation, the variation of the velocity, temperature, species, and passives in a grid cell are referred to determine whether the cell is embedded or the embedding should be removed [7]. At present, Eulerian –Lagrangian method is widely used to simulate the spray and atomization. As a result, the spray simulation has a high grid resolution dependency. The simulated liquid penetration increases with a decrease in the grid size, but does not converge to the experimental data. Over-small grid size will lead to an over-prediction of the liquid penetration [27]. AMR technique is one of methods to optimize the grid resolution and eliminate the grid resolution dependency. As shown in Figure 2, the spray structure is quite different for each grid resolution used. In the cases of the grid resolutions of 2.0×2.0 mm and 1.0×1.0 mm, the spray shape is not reasonable compared to the experimental observations. Reasonable spray shapes are obtained for both the fine grid (0.5×0.5 mm) and the AMR methods, respectively. Therefore, the AMR method with a minimum grid size of 0.25×0.25 mm is implemented to refine the grid and save computational costs.

5 Results and Discussion

5.1 Effect of breakup models on the spray simulation in a constant volume vessel

During this part of the present study, the fuel spays are considered injected into a constant volume vessel having a gas medium at the conditions given in Table 4. The simulated results are

compared to the experimental results [16], in an attempt to assess the predictive capability of the various breakup models. The fuel used in the experiment is a mixture of n-decane, naphthalene (Np) and tetramethyl-p-phenylene diamine (TMPD) in a mass proportion of 90:9:1, and the TMPD is used for its fluorescence characteristics in the PLIEF measurement technique [16]. In the present simulation study, the mixture of 91% n-decane and 9% naphthalene in the mass fraction is used. The breakup models evaluated are listed in Table 5.

Figure 3 shows a comparison of the liquid spray penetration between the present model predictions and the measured results taken from [16]. It is seen that all the spray breakup models have the same prediction for the liquid spray penetration in the initial injection period, but then behave quite differently for the succeeding period in which the experimental liquid spray tip penetration remains an almost constant. The three TAB based models (TAB, TAB-CHI and TAB-RR) significantly underpredict the liquid spray tip penetration. The drop size distribution in the TAB model makes only a slight difference in the prediction of the liquid spray tip penetration. For the KH-RT hybrid model, the liquid breakup length has a significant influence in the predictive capability for the liquid spray penetration because the breakup length is proportional to the breakup time τ_{KH} which is shown in eq. (14). The predicted spray liquid penetration increases with an increase in the breakup time. The results show that the predicted penetration using the KH-RT model with the breakup length constant $C_{bl} = 10$ in eq. (20) agrees with the experimental data reasonably well. Also, the modified KH-RT model in which a specific breakup length is removed provides a predicted result which is in reasonable agreement with the experimental data. The RT model significantly underpredicts the liquid penetration. This suggests that such mechanism breaks up droplets too fast if it is used for the earlier stage of the spray development. However, in the initial fuel injection period, all models have a shorter

predicted penetration compared to the experimental results. This behavior may occur because the relative measurement error in the initial injection period is higher than that in the later stage of the injection period. It is also observed that the liquid spray penetration predicted by all the models increases initially, reaches a peak value, and then reduces to an asymptotic constant, except for the KH-RT model with the breakup length constant of $C_{bl} = 20$, this is because these models predict small droplets in the spray tip region, which vaporizes in the high temperature gas environment, resulting in the peak value in the penetration. The long breakup length predicted by the KH-RT model with the breakup length constant of $C_{bl} = 10$ predicts unreasonable spray penetration as well as other spray characteristics as shown in Figures 5 and 6 and explained below.

Shown in Figure 4 is a comparison of the liquid phase sprays predicted by the present simulation employing the various breakup models given in Table 5 against the experimental results [16]. It is clear that the predicted liquid phase spray is significantly influenced by the breakup models used in the numerical simulation. The modified KH-RT model provides a reasonable simulation result. For the KH-RT model, the predicted liquid phase spray is very sensitive to the numerical value of the breakup length constant C_{bl} appeared in eq. (20). The KH-RT model with $C_{bl} = 10$ provides a reasonable predicted results. However, using $C_{bl} = 20$ leads to a longer breakup time τ_{KH} , and a longer penetration; even the overall characteristics of the liquid phase spray deviate considerably from the experimental observations. Further, it can be seen that all three TAB based models under-predict both spray angle and spray tip penetration for the liquid phase.

A comparison with the experimental results is given in Figure 5 for the simulated vapour phase spray based on the seven breakup models considered in this study. The numerical results are presented in terms of the contour plots for the equivalence ratio, similar to the experimental

results [16]. The equivalence ratio is determined by the competition between the rate of local fuel evaporation and the ambient gas entrainment, and the latter is related to the liquid breakup, penetration and turbulent transport. However, overall the vapour phase distribution is more like a turbulent jet injected into a stationary medium, as shown in Figure 5. It can be observed that the effect of the breakup model on the vapour phase simulation is much smaller than that on the liquid phase simulation discussed earlier. All model predictions of the vapour phase shape, except the KH-RT model with $C_{bl} = 20$, agree reasonably with the experimental measurements for the vapour phase. This might be attributed to two reasons: first, it can be seen from Figure 6 that for various liquid breakup models, except the KH-RT model with $C_{bl} = 20$, the predicted liquid spray mass which remains in the constant-volume vessel is very similar for the sprays investigated, although the simulated liquid-phase shape of the injected fuel is quite different among various liquid breakup models studied. This suggests that various liquid breakup models used, except the KH-RT model with $C_{bl} = 20$, predict the similar amount of vapour-phase fuel which is derived from the injected liquid-phase fuel. Second, the numerical results of the isosurface of the turbulent kinetic energy of the ambient flow, as illustrated in Figure 7, indicate that the model constant C_{bl} in the KH-RT model and the drop size distribution in the TAB model have a quite small effect on the turbulent kinetic energy of the ambient gas. Therefore, similar vapour-mass and turbulent kinetic energy are predicted using the various liquid breakup models, except the KH-RT model with $C_{bl} = 20$.

5.2 Effect of breakup models on the engine simulation

The numerical simulations are implemented to clarify the predictive capability of the breakup models, for engine simulations by comparing the numerical results with the engine test data

carried out by Klingbeil et al. [17] in a single cylinder high pressure direct injection diesel engine, The engine operating conditions are shown in Table 6.

The results of the present numerical simulation implementing various liquid breakup models are compared in Figure 8 against the experimental engine test results [17]. For the measured and simulated in-cylinder pressure histories shown in Fig. 8(a), it is seen that the modified KH-RT model, the KH-RT model with $C_{bl} = 10$ and RT model provide the simulated results that are in good agreement with the experimental results. The KH-RT model with $C_{bl} = 20$ significantly under-predicts the in-cylinder pressure. Three TAB based models have a similar prediction of the in-cylinder pressure which is lower than the experimental data. The experimental and numerical heat release rates shown in Figure 8(b) indicate that all three kinds of TAB models and the KH-RT model with $C_{bl} = 20$ predict a significantly small premixed combustion phase and a quite large diffusive combustion phase. The predicted heat release rates using the KH-RT model with $C_{bl} = 10$ and the RT model are close to the experimental data, but a little lower. It also can be seen that the modified KH-RT model can predict the heat release rate reasonably, being in better agreement with the experimental results.

Figure 9 illustrates the simulated distribution of the in-cylinder equivalence ratio and spray at the crank angle of -5° ATDC. It can be observed that the RT model and all three TAB based models predict a shorter spray penetration compared to the modified KH-RT model. As a result, their spray cannot impact the combustion chamber. The high equivalence ratio areas of all three TAB models are close to the injector due to their overprediction of droplet breakup. The KH-RT model with $C_{bl} = 20$ significantly underpredicts droplet breakup, leading to a long predicted spray penetration. It is found that for the KH-RT model, the breakup length constant, C_{bl} ,

strongly affects the simulated results of the spray and atomization process and hence the mixture formation process as well.

A comparison of the soot and NO_x emissions is shown in Figure 10 between the present simulated results using various liquid breakup models and the experimental results made by Klingbeil, et al. [17]. The soot emission predicted by the modified KH-RT model and the RT model are in a good agreement with the experimental results at the engine-out point. All three TAB models and the KH-RT model with $C_{bl} = 10$ overpredict the soot emission, while The KH-RT model with $C_{bl} = 20$ predicts an obviously unreasonable soot emission result compared to the experimental data at the engine-out point. For the NO_x emission, only the prediction using the modified KH-RT model matches the experimental results well at the engine-out point, while the RT model overpredicts and the TAB models and the KH-RT model with $C_{bl} = 10$ and 20 underpredict the engine-out NO_x emission considerably. It is seen that some model yields good prediction for NO_x emission while others yields good prediction for soot emission; however, only the modified KH-RT model provides good prediction for both NO_x and Soot emission simultaneously.

6 Conclusions

In this study the effect of various liquid breakup models has been investigated on the simulated characteristics of high-pressure fuel sprays injected into a high pressure and high temperature ambience in a constant volume vessel and on the simulated engine performance for a high-pressure DI diesel engine. The results indicate that the modified Kelvin-Helmholtz – Rayleigh-Taylor (KH-RT) breakup model, in which the fixed breakup length is removed, gives the most reasonable predicted results in both engine simulation and constant-volume vessel spray

simulation. For the standard KH-RT model, the model constant C_{bl} has a significant effect on the model's predictability, and a fixed value of the constant C_{bl} cannot provide a satisfactory result for different operation conditions. All three Taylor-Analogy-Breakup (TAB) based models predict a quite small premixed combustion phase and a large diffusive combustion phase due to their overprediction of droplet breakup. The RT model is not appropriate to be used as a single model in a diesel-like fuel spray simulation.

7 Acknowledgements

This work is supported financially by the Ontario Research Fund-Research Excellence (ORF-RE) program via contract # RE-02-019 and the Natural Sciences and Engineering Research Council of Canada (NSERC) via a Discovery Grant. Convergent Science is gratefully acknowledged for providing their Converge™ CFD code for the present study.

References

- [1] M. Badami, P. Nuccio, G. Trucco, Influence of Injection Pressure on the Performance of a DI Diesel Engine with a Common Rail Fuel Injection System, SAE Paper (1999) 1999-01-0193.
- [2] C. Baumgarten, Mixture Formation in Internal Combustion Engines, Springer, Berlin, 2006.
- [3] E.C. Felice, M.V. Bianca, E.C. Giuseppe, Potential of Multiple Injection Strategy for Low Emission Diesel Engines, SAE Paper (2002) 2002-01-1150.
- [4] R.D. Reitz, Modeling Atomization Processes in High-pressure Vaporizing Sprays, Atomization and Spray Technology 3(4) (1987) 309-337.
- [5] R.D. Reitz, F.V. Bracco, Mechanism of Breakup of Round Liquid Jets, The Encyclopedia of Fluid mechanics, Chermisnoff N (ed), Gulf Publishing, Houston, TX, 3 (1986) 233-249.
- [6] G.I. Taylor, The Instability of Liquid Surfaces when Accelerated in a Direction Perpendicular to their Planes, Batchelor GK, The Scientific Papers of GI Taylor, University Press, Cambridge, 33 (1950) 532-536.

- [7] P.K. Senecal, K.J. Richard, E. Pomraning, A New Parallel Cut-cell Cartesian CFD Code for Rapid Grid Generation Applied to In-cylinder Diesel Engine Simulations, SAE Paper (2007) 2007-01-0159.
- [8] P.K. Senecal, Development of a Methodology for Internal Combustion Engine Design Using Multi-Dimensional Modeling with Validation Through Experiments, Ph.D. Thesis, Dept. of Mechanical Engineering, University of Wisconsin-Madison, 2000.
- [9] P.J. O'Rourke, A.A. Amsden, The TAB Method for Numerical Calculation of Spray Droplet Breakup, SAE Paper (1987) No. 872089.
- [10] P.J. O'Rourke, A.A. Amsden, A Spray/Wall Interaction Submodel for the KIVA-3 Wall Film Model, SAE Paper (2000) 2000-01-0271.
- [11] D.P. Schmidt, C.J. Rutland, A New Droplet Collision Algorithm, Journal of Computational Physics 164 (1) (2000) 62-80.
- [12] K. Sone, S. Menon, Effect of Subgrid Modeling on the In-Cylinder Unsteady Mixing Process in a Direct Injection Engine, J. Eng. Gas Turbines Power 125(2) (2003) 435-443.
- [13] T. Hori, J. Senda, T. Kuge, H. Fujimoto, Large Eddy Simulation of Non-Evaporative and Evaporative Diesel Spray in Constant Volume Vessel by Use of KIVALES, SAE Paper (2006) 2006-01-3334.
- [14] M. Larimi, J. Tiainen, Diesel Spray Simulation and KH-RT Wave Model, SAE Paper (2003) 2003-01-3231.
- [15] H. Fujimoto, T. Hori, J. Senda, Effect of Breakup Model on Diesel Spray Structure Simulated by Large Eddy Simulation, SAE Paper (2009) 2009-24-0024.
- [16] W. Su, T. Sun, H. Guo, Quantitative Study of Concentration and Temperature of a Diesel Spray by Using Planar Laser Induced Exciplex Fluorescence Technique, SAE Paper (2010) 2010-01-0878.
- [17] A.E. Klingbeil, H. Juneja, Y. Ra, Premixed Diesel Combustion Analysis in a Heavy-Duty Diesel Engine, SAE Paper (2003) 2003-01-0341.
- [18] Z. Han, R.D. Reitz, Turbulence Modeling of Internal Combustion Engines Using RNG κ - ϵ Models, Combust. Sci. and Tech. 106(4-6) (1995) 267-295.
- [19] B.E. Launder, D.B. Spalding, Lectures in Mathematical Models of Turbulence, Academic Press, 1972.
- [20] V. Yakhot, L.M. Smith, The Renormalization Group, the E-expansion and Derivation of Turbulence Models, J. Sci. Comput. 7 (1992) 35-61.

- [21] Y. Ren, X.G. Li, Numerical study on combustion and emissions characteristics of a direct injection (DI) diesel engine, Proceedings of Combustion Institute – Canadian Section (2009) 18-23.
- [22] C.H. Chiang, M.S. Raju, W.A. Sirignano, Numerical Analysis of a Convecting, Vaporizing Fuel Droplet with Variable Properties, Int. J. Heat Mass Transfer 35(5) (1992) 1307-1324.
- [23] J. Xin, D.T. Montgomery, Z. Han, R.D. Reitz, Computer Modeling of the Six-Mode Emissions Test Cycle of a DI Diesel Engine, Journal of Engineering for Gas Turbines and Power 119 (1997) 683-691.
- [24] H. Hiroyasu, T. Kadota, Models for Combustion and Formation of Nitric Oxide and Soot in Direct Injection Diesel Engines, SAE Paper (1976) No.760129.
- [25] J. Nagle, R.F. Strickland-Constable, Oxidation of carbon between 1000-2000 C, Proc. of the Fifth Carbon Conf. 1 (1962) 154-164.
- [26] D.C. Wilcox, Turbulence Modeling for CFD, DCW Industries, California,. USA , 1994
- [27] N. Abani, A. Munnannur, R. D. Reitz, Reduction of Numerical Parameter Dependencies in Diesel Spray Models. Trans. ASME, J. Engng Gas Turbines Power 130 (2002) 032809-1-9.

Table 1 Engine specifications [17]

Engine	Caterpillar 3401E SCOTE(Single Cylinder Oil Test Engine)
Bore x Stroke (mm)	137.2 x 165.1
Compression Ratio	16.1:1
Displacement (L)	2.44
Connecting Rod Length (mm)	261.6
Squish Height (mm)	1.57
Intake Valve Closing	-143 Degree ATDC
Exhaust Valve Opening	130 Degree ATDC

Table 2 Injection system parameters [17]

Injector Type	Electronic Unit Injector (EUI)
Maximum Injection Pressure (MPa)	190
Number of Nozzle Holes	6
Nozzle Hole Diameter (mm)	0.214
Included Spray Angle	130°
Injection Rate Shape	Rising

Table 3 The other sub-models implemented in this study

<u>Physical process</u>	<u>Model</u>
Drop collision	NTC model [11]
Drop turbulent dispersion	O'Rourke turbulent dispersion model
Drop vaporization	Amsden-Chiang model [22]
Ignition and Combustion (Only used in the engine simulation)	Shell + Characteristic Time Combustion (CTC) Model [23]
Pollutant formation (Only used in the engine simulation)	Extended Zel'dovich model & Hiroyasu-NSC oxidation soot model [24, 25]

Table 4 Conditions for fuel sprays injected into a constant volume vessel considered in this study

Injection pressure (MPa)	180
Injection duration (ms)	1.0
Ambient temperature (K)	950
Ambient density (kg/m ³)	60
Injector diameter D_n (mm)	0.1

Table 5 Various breakup models evaluated in the present study

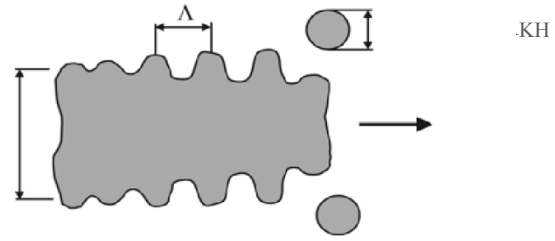
Case	Breakup Model
1	Kelvin-Helmholtz (KH) - Rayleigh-Taylor (RT) modified model
2	KH-RT model with the breakup length constant $C_{bl}=10$ in eq. (20)
3	KH-RT model with $C_{bl} = 20$ in eq. (20)
4	KH-RT model with $C_{bl} = 40$ in eq. (20)
5	Taylor-Analogy-Breakup (TAB) model (without the drop size distribution)
6	TAB-CHI model (with the chi-squared drop size distribution)
7	TAB-RR model (with the Rosin-Rammler drop size distribution)

Table 6 Engine operating conditions for experimental study carried out by Klingbeil, et al. [17]

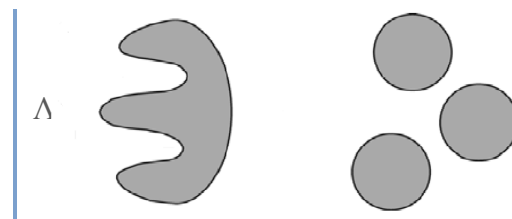
Engine Speed	821
Start of Injection	-9° ATDC
Injection Duration	5.5°
EGR (%)	48.34
Intake Pressure (KPa)	103
Intake Temperature (K)	393

Figure Captions

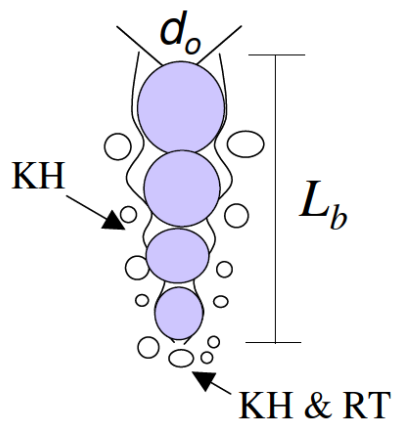
- Fig. 1 Schematic of the various liquid breakup models considered in this study [2]: (a) Kelvin-Helmholtz (KH) model, (b) Rayleigh-Taylor (RT) model, and KH-RT hybrid model
- Fig. 2 Grid resolutions (a) and the corresponding simulated results (b) using the KH-RT hybrid breakup model for sprays injected into the constant-volume vessel. The experimental image is taken from [16]
- Fig. 3 A comparison of the predicted and measured liquid spray tip penetration for fuel injected into the constant-volume vessel. The measured data is taken from [16]. Ambient gas temperature $T_a = 950$ K and ambient gas density $\rho_a = 60 \text{ kg/ m}^3$
- Fig. 4 Simulated results of the liquid phase spray in the constant-volume vessel. The ambient gas temperature is $T_a = 950$ K, ambient gas density is $\rho_a = 60 \text{ kg/ m}^3$ and the injection time is 0.5 ms after the start of injection
- Fig. 5 Simulated results of the vapour phase spray in the constant-volume vessel. The ambient gas temperature is $T_a = 950$ K, ambient gas density is $\rho_a = 60 \text{ kg/ m}^3$ and the injection time is 0.5 ms after the start of injection
- Fig. 6 Simulated results of the liquid spray mass in the constant-volume vessel. The ambient gas temperature is $T_a = 950$ K and ambient gas density is $\rho_a = 60 \text{ kg/ m}^3$
- Fig. 7 Effect of the liquid breakup models on the numerical results for the isosurface of the turbulent kinetic energy (κ , $\kappa = 150 \text{ J/kg}$) of the ambient gas in the constant-volume vessel
- Fig. 8 Comparison between the present numerical simulation employing various liquid breakup models and the experimental results by Klingbeil, et al. [17]: (a) in-cylinder pressure history, and (b) heat release rates (HRR)
- Fig. 9 Numerically simulated distributions of the in-cylinder equivalence ratio and simulated in-cylinder spray at the crank angle of -5° ATDC
- Fig. 10 Comparison of the soot and NO_x emissions between the present numerical simulation employing various liquid breakup models and the experimental results by Klingbeil, et al. [17]



(a)



(b)



(c)

Fig. 1 Schematic of the various liquid breakup models considered in this study [2]: (a) Kelvin-Helmholtz (KH) model, (b) Rayleigh-Taylor (RT) model, and KH-RT hybrid model

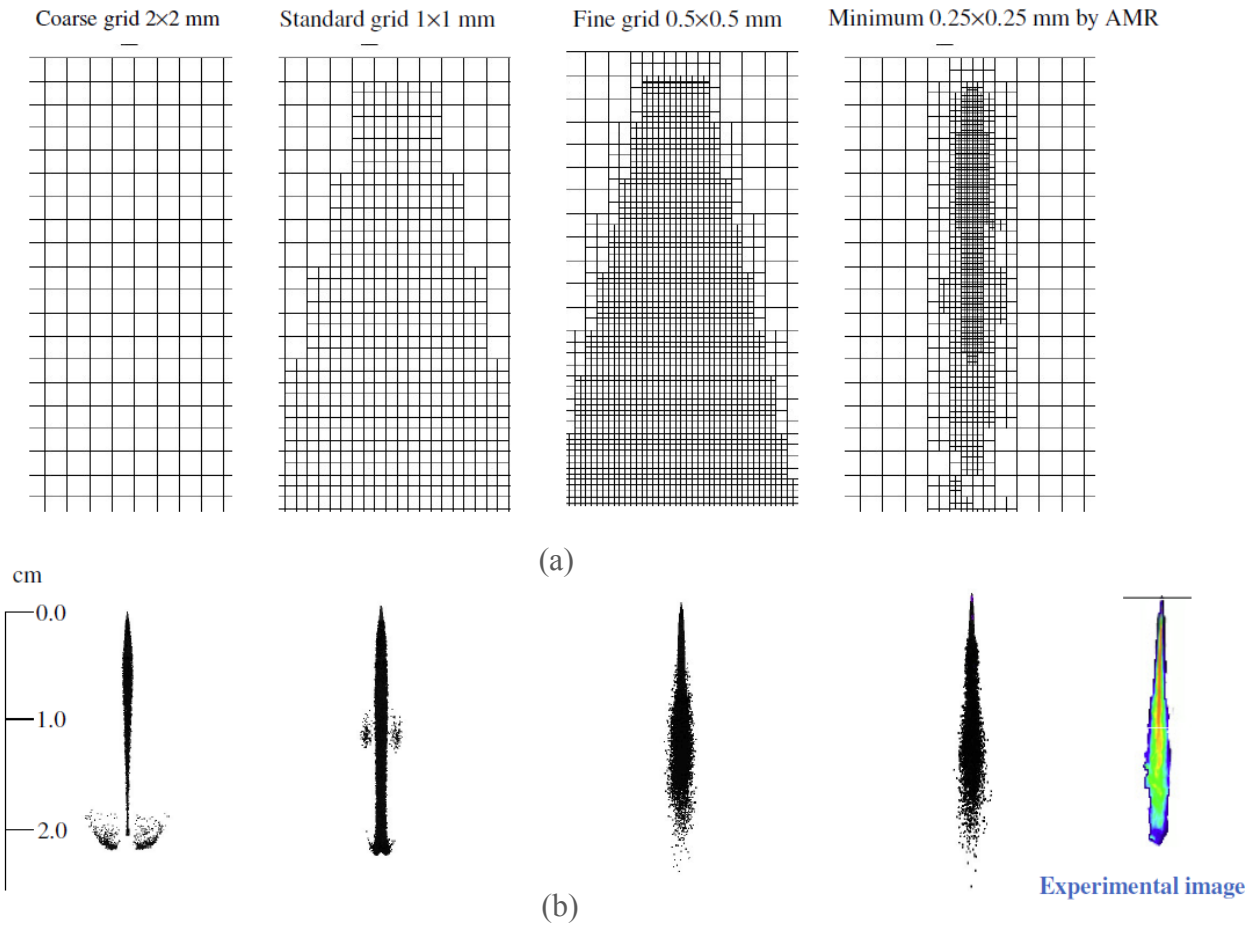


Fig. 2 Grid resolutions (a) and the corresponding simulated results (b) using the KH-RT hybrid breakup model for sprays injected into the constant-volume vessel. The experimental image is taken from [16]

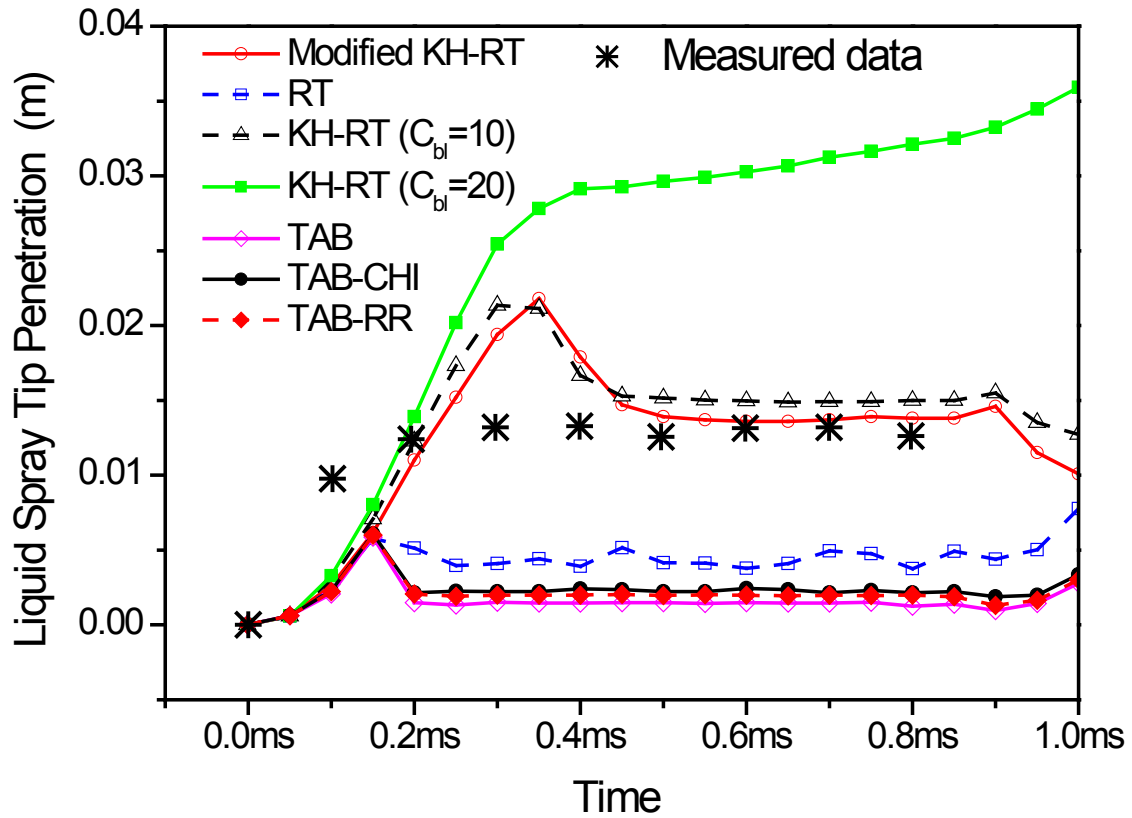


Fig. 3 A comparison of the predicted and measured liquid spray tip penetration for fuel injected into the constant-volume vessel. The measured data is taken from [16]. Ambient gas temperature $T_a = 950$ K and ambient gas density $\rho_a = 60\text{kg/m}^3$

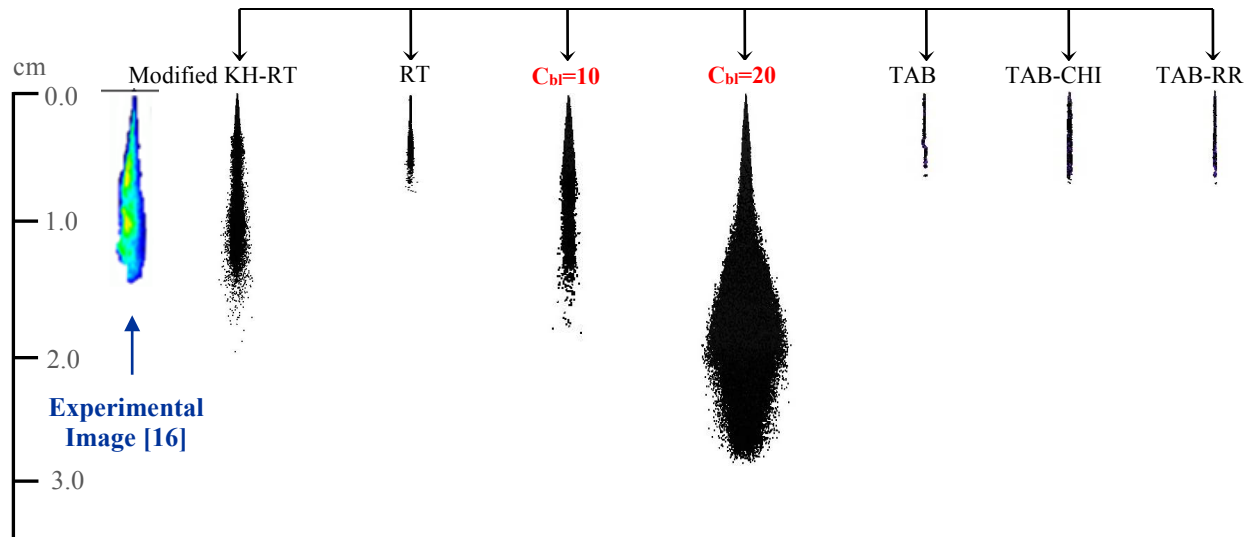


Fig. 4 Simulated results of the liquid phase spray in the constant-volume vessel. The ambient gas temperature is $T_a = 950$ K, ambient gas density is $\rho_a = 60$ kg/ m³ and the injection time is 0.5 ms after the start of injection

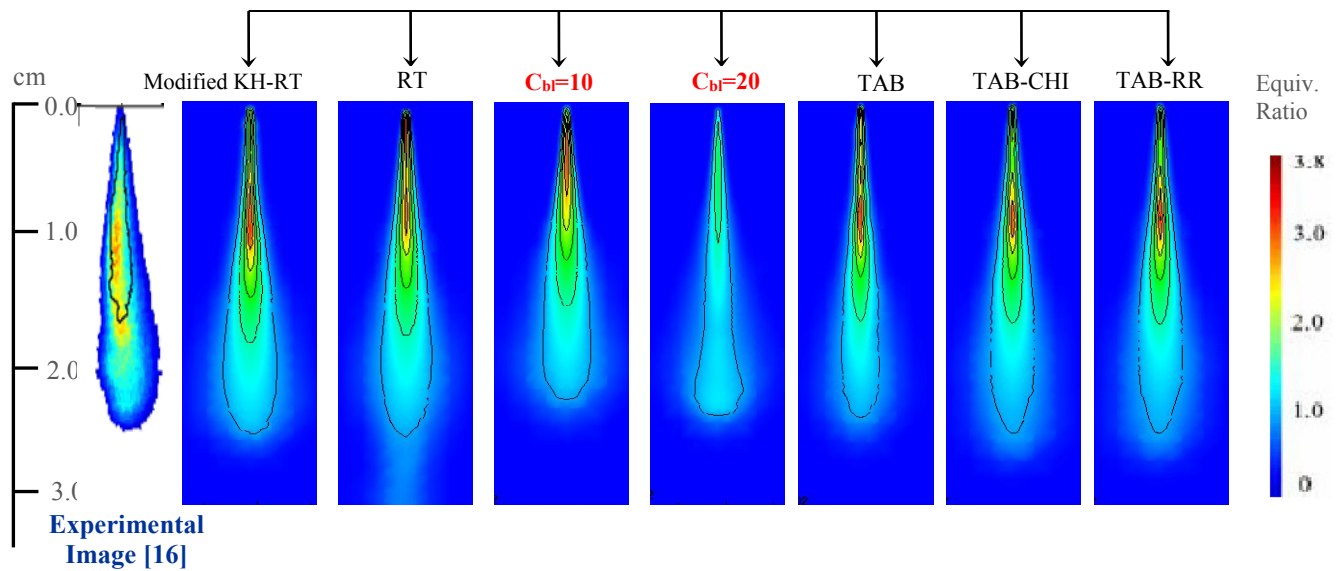


Fig. 5 Simulated results of the vapour phase spray in the constant-volume vessel. The ambient gas temperature is $T_a = 950$ K, ambient gas density is $\rho_a = 60$ kg/ m³ and the injection time is 0.5 ms after the start of injection

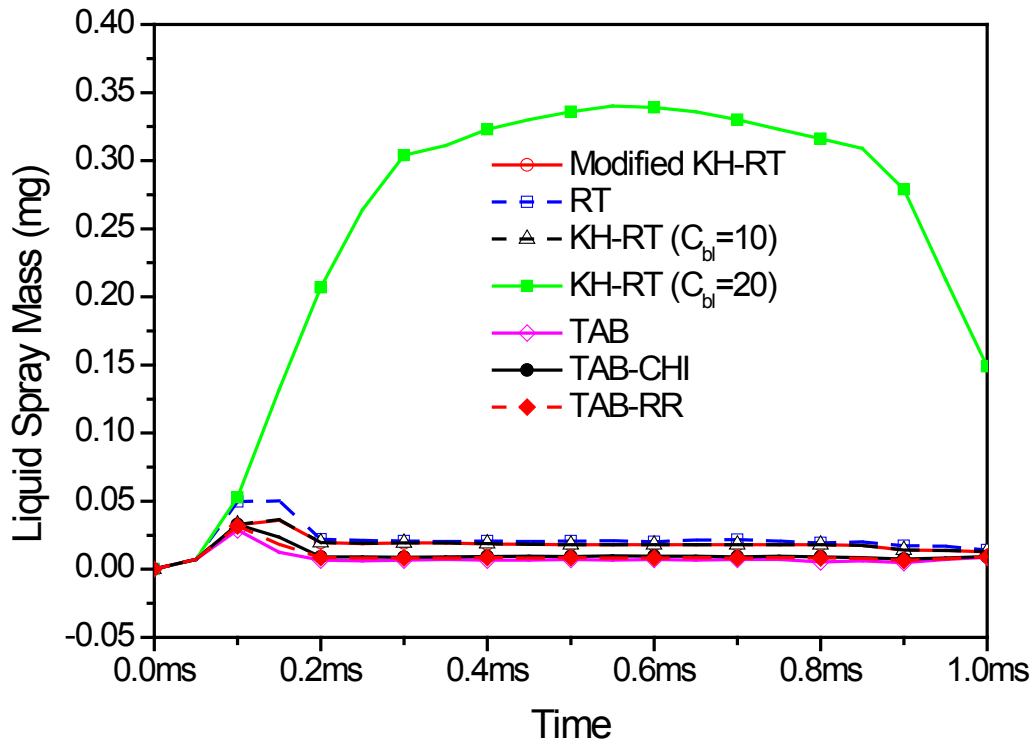


Fig. 6 Simulated results of the liquid spray mass in the constant-volume vessel. The ambient gas temperature is $T_a = 950$ K and ambient gas density is $\rho_a = 60$ kg/ m³

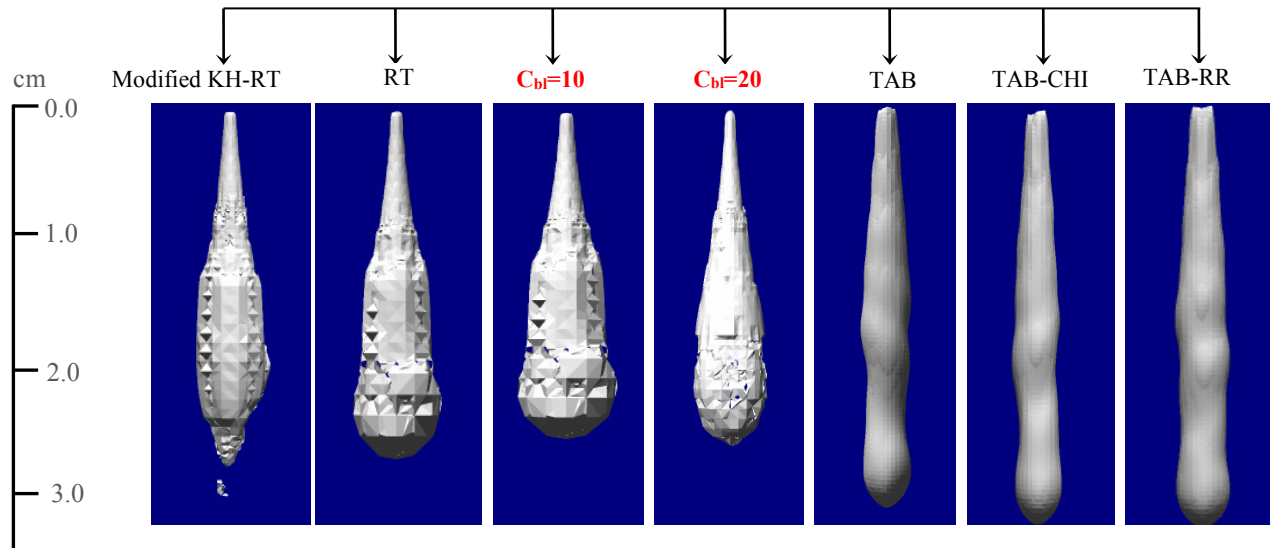
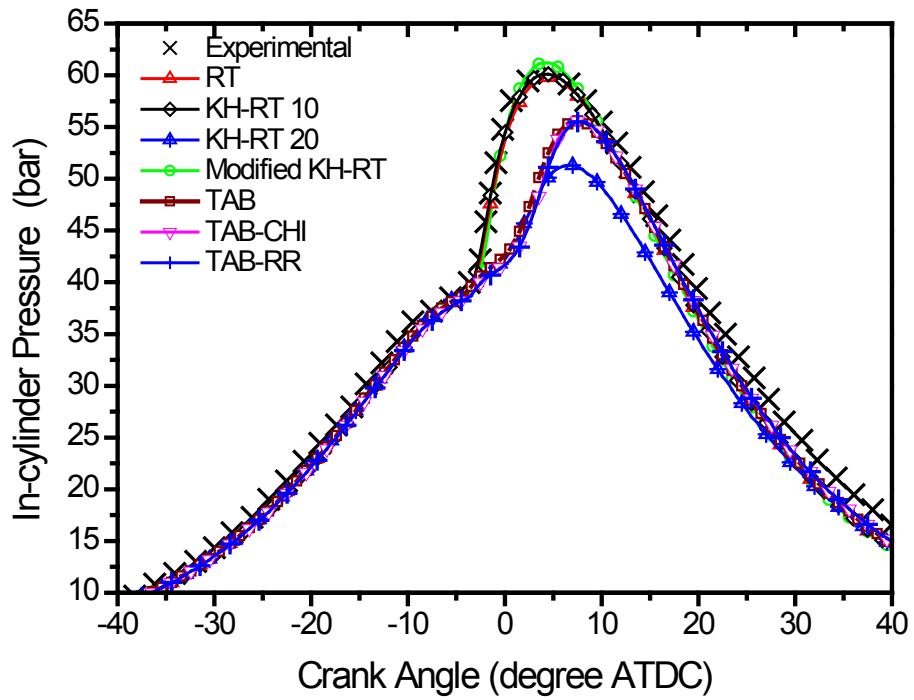
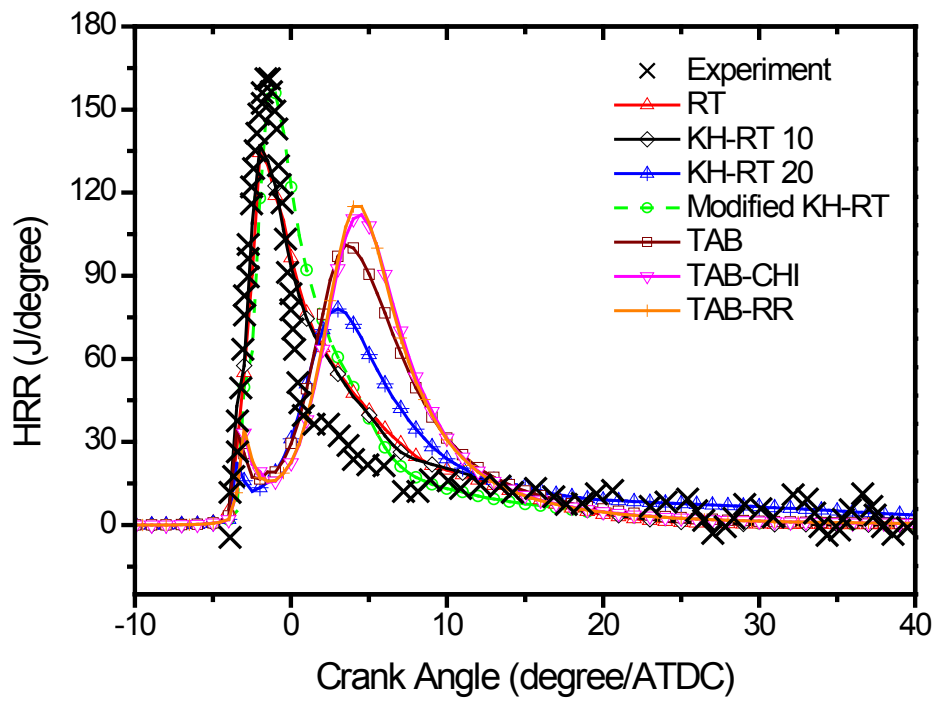


Fig. 7 Effect of the liquid breakup models on the numerical results for the isosurface of the turbulent kinetic energy (κ , $\kappa = 150$ J/kg) of the ambient gas in the constant-volume vessel



(a)



(b)

Fig. 8 Comparison between the present numerical simulation employing various liquid breakup models and the experimental results by Klingbeil, et al. [17]: (a) in-cylinder pressure history, and (b) heat release rates (HRR)

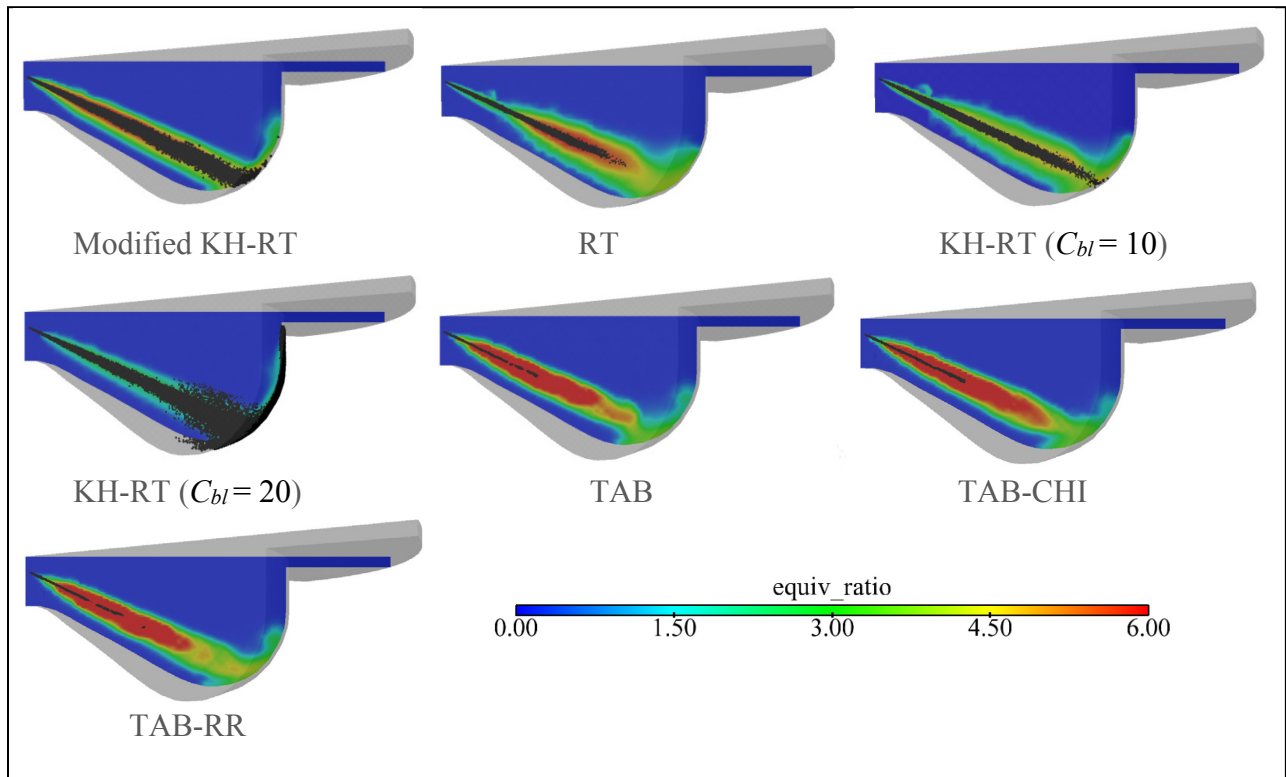


Fig. 9 Numerically simulated distributions of the in-cylinder equivalence ratio and simulated in-cylinder spray at the crank angle of -5° ATDC

Fig. 10 Comparison of the soot and NO_x emissions between the present numerical simulation employing various liquid breakup models and the experimental results by Klingbeil, et al. [17]

